ChemComm

Accepted Manuscript

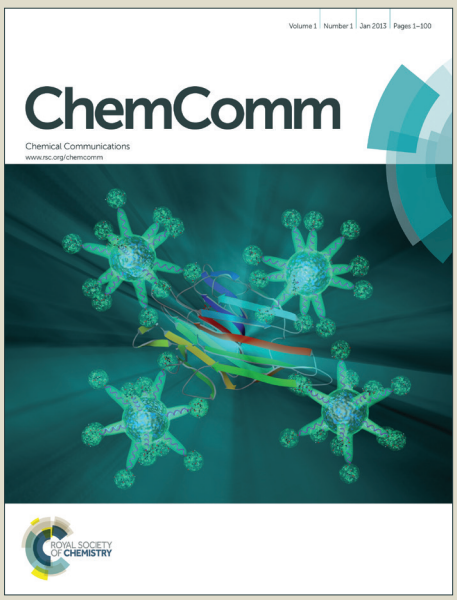

ROYAL SOCIETY OF CHEMISTRY

www.rsc.org/chemcomm

Journal Name RSCPublishing

COMMUNICATION

Synthetic Control of Composition and Crystallite Size of Silver Ferrite Composites: Profound Electrochemistry Impacts

Cite this: DOI: 10.1039/x0xx00000x

Received 00th January 2012,
Accepted 00th January 2012

DOI: 10.1039/x0xx00000x

www.rsc.org/

Jessica L. Durham,[a] Kevin Kirshenbaum,[b] Esther S. Takeuchi,[a,b,c] Amy C. Marschilok,[a,c] Kenneth J. Takeuchi,[a,c*]

A paradigm for concomitant control of crystallite size and composition of bimetallic composites via co-precipitation is introduced. Direct preparation of composites of silver ferrite and amorphous maghemite via nonstoichiometric synthesis was demonstrated. Notable impact on electrochemistry was observed, with ~200% increase in reversible capacity for the small crystallite material.

Silver ferrite, $AgFeO_2$, exhibits a layered delafossite-type structure with the general chemical formula ABO_2. Ternary delafossites (ABO_2) contain alternating layers of edge-shared BO_6 octahedra, where the B cation site can incorporate a variety of trivalent transition metal cations (i.e. Fe^{3+}) with close-packed monovalent A^+ metal cations (i.e. Ag^+) located between the layers.[1] The synthesis of silver ferrite was first reported in the early 1930s;[2] to date, synthetic strategies employed to produce ternary delafossite-type oxides have included high-temperature, hydrothermal, solid state, cation exchange, and microwave or ultrasonic irradiation.[3] An initial reflux based synthesis reported in 2012 demonstrated the feasibility of low-temperature synthesis of pure stoichiometric $AgFeO_2$.[4] Synthesis from non-stoichiometric compositions of Ag^+ and Fe^{3+} nitrate was described in 2013, where the non-stoichiometric reactant ratios produced mixtures of products, including Ag_2O and α-FeOOH.[5]

The layered structure of delafossites enables ion transport and copper based delafossites have been explored for energy storage applications.[6] A limited number of literature reports describe exploration of silver delafossite oxides as cathodes in lithium based batteries, including an investigation of $AgCuO_2$ and $AgCu_{0.5}Mn_{0.5}O_2$.[7] Preliminary studies of $AgFeO_2$ demonstrate that stoichiometric silver ferrite, with an Ag:Fe ratio of 1:1 and an average crystallite size of 31 nm, is electrochemically active.[4]

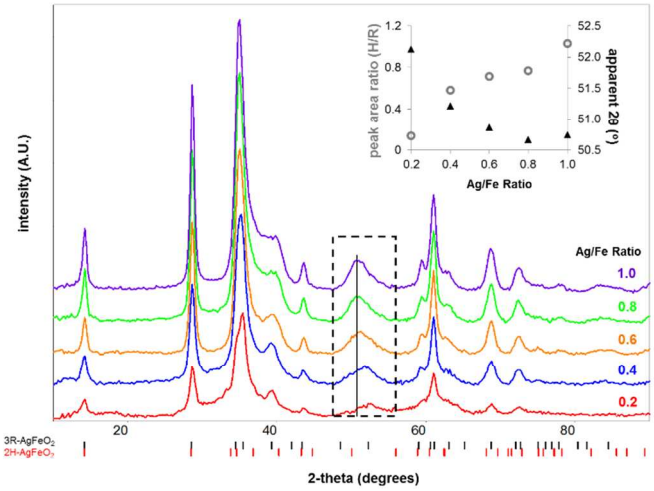

Figure 1. X-ray powder diffraction of silver ferrite. Reference patterns for 3R (01-075-2147) and 2H (01-070-1452) polytypes. Dotted region used for inset.

Our previous studies of crystallite size control of magnetite (Fe_3O_4) and silver hollandite ($Ag_xMn_8O_{16}$) provided fundamental crystal size / electrochemistry insight, along with a notable increase in cycling capacity with smaller crystallite size.[8] We hypothesized that silver ferrite crystallite size control would be possible synthetically, **Figure 1**. Further, we anticipated a crystal size / electrochemistry relationship with silver ferrite reminiscent of magnetite and silver hollandite. The critical discovery with this study is the synthesis and electrochemistry of a composite consisting of nanocrystalline silver ferrite and amorphous maghemite.

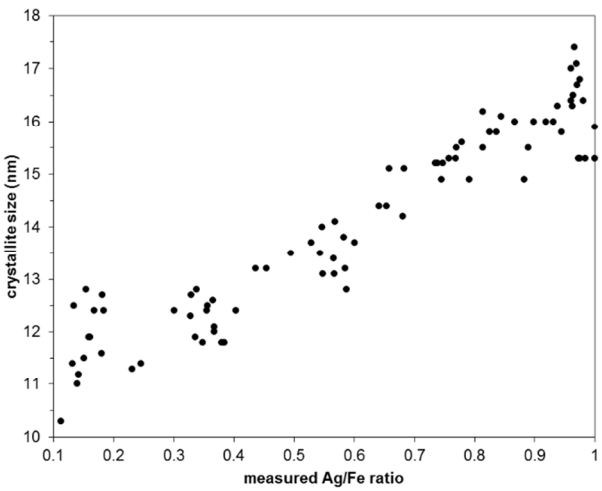

Figure 2. Crystallite size versus measured Ag/Fe ratio in as prepared samples.

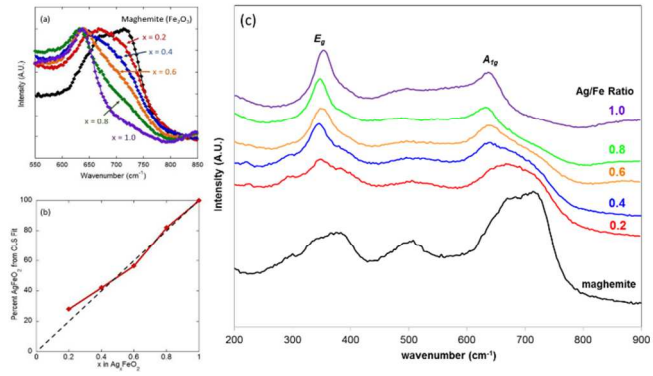

Figure 3. Raman spectroscopy of as prepared samples and maghemite reference material. **a.** Intensity vs. wavenumber for A_{1g} region (550 – 850 cm^{-1}). **b.** Percent $AgFeO_2$ vs. Ag/Fe ratio from linear combination fit. **c.** Intensity vs. wavenumber for full scan (200 – 900 cm^{-1}).

Silver ferrite was synthesized via a co-precipitation reaction with reagent mixtures containing Ag/Fe ratios ranging between 0.2 and 1.0 using the method previously reported for preparation of stoichiometric $AgFeO_2$.[4] The abbreviation Ag_xFeO_2, where x = Ag content, is used here for simplicity. Inductively coupled plasma optical emission spectroscopy was used to measure silver and iron content of the samples and the product ratios reflected the reaction ratios, **Figure 2.**

The silver ferrite samples so produced displayed XRD spectra consistent with $AgFeO_2$ reference patterns, **Figure 1**. Notably, the diffraction patterns do not show presence of metallic silver or additional impurities (e.g. Ag_2O, FeOOH) commonly reported during delafossite synthesis.[9] As the Ag/Fe ratio decreases, peak broadening is observed consistent with reduction of the crystallite size. The decrease in crystallite size is accompanied by an increase in surface area which systematically increases from 50 m^2/g to 250 m^2/g for the 1.0 and 0.2 Ag/Fe samples, respectively. Close examination of the XRD patterns shows that the peak maximum at ~50 - 52° 2θ appears to shift with changing composition, **Figure 1 inset, primary axis.** For the rhombohedral (3R) phase, the peak at 52° two theta is a reflection of the (0 1 8) plane directly bisecting silver, oxygen, and iron. For the hexagonal (2H) phase, the peak at 50° two theta is a reflection of the (1 0 5) plane directly bisecting iron and slightly bisecting silver and oxygen. By locking the two theta positions at the (0 1 8) and (1 0 5) peak positions for these two $AgFeO_2$ phases, linear combination fitting was used to determine the ratios of the peak areas in the 50 – 52° 2 theta range for the 3R and 2H phases, **Figure 1 inset, secondary axis**. The fits indicate that the low silver material is primarily 3R phase, while the stoichiometric material is approximately equal amounts of 3R and 2H.

Raman data of silver ferrite has been published previously in which E_g and A_{1g} peaks are observed at 345 and 638 cm^{-1}, respectively, **Figure 3**.[9d] The stoichiometric $AgFeO_2$ (Ag/Fe = 1.0) material prepared via co-precipitation demonstrates peaks at 350 and 631 cm^{-1}, respectively, consistent with the E_g and A_{1g} literature values, **Figure 3c**. As the Ag/Fe ratio decreases, Raman spectra continue to demonstrate intrinsic silver ferrite peaks while shoulders detected at 285, 374, and 707 cm^{-1} increase as the silver content decreases **Figure 3a**. The E_g and A_{1g} peaks in the vibrational spectrum of the delafossite are attributed to fundamental bond distances, energies, and angles of the delafossite structure, do not change in position or relative intensity, suggesting that the silver ferrite structure remains intact throughout the series of silver ferrite products. The peaks at 285, 374, and 707 cm^{-1} appear among the low silver content samples, **Figure 3c**, and are reminiscent of the Raman spectrum of maghemite (γ-Fe_2O_3).[10] Using the maghemite and x = 1.0 spectra as references, classical least squares (CLS) fitting was used to determine the contribution of the reference spectra to a mixed component spectrum. The percent contribution of the $AgFeO_2$ reference spectrum was found to decrease linearly as the Ag content decreased, **Figure 3b**, where the percent $AgFeO_2$ in each spectrum matched the silver content in each material (dashed line). These results suggest that a combination of $AgFeO_2$ and γ-Fe_2O_3 are present rather than a solid solution of Ag_xFeO_2 with Ag vacancies. These results are in agreement with the XRD results which show that the lattice constants do not change as a function of silver content, as would be expected in a crystal structure with up to 80% vacancies on one site. The maghemite, while clearly visible in the Raman spectra, is not detected by XRD, consistent with amorphous maghemite.

The results suggest a direct synthesis of a composite comprised of crystalline silver ferrite ($AgFeO_2$) and non-crystalline maghemite (γ-Fe_2O_3). One interpretation of the evidence is the formation of a layer of non-crystalline maghemite on the surface of the crystalline silver ferrite. During the synthetic process, the growth of the $AgFeO_2$ in the smaller crystallite materials may be limited by the deprivation of silver ions in the reaction mixture; thus, the smaller crystallite silver ferrites may be comprised of a core of silver ferrite and surface layer of maghemite. Scanning electron micrographs of each material indicate aggregates of 1 to 5 microns at all Ag/Fe ratios, Figure S1.

The sensitivity of XANES (x-ray absorption near edge structure) to oxidation state and coordination number provided a useful complement to characterization of the nanocrystalline materials by XRD and Raman. Iron K-edge and silver K-edge data were collected and compared with a variety of reference materials (metallic Fe, FeO, Fe_3O_4, and Fe_2O_3 for iron; metallic Ag and Ag_2O for silver). The Fe K-edges for the various silver ferrite samples were all nearly equivalent to the absorbance spectrum of Fe_2O_3 with edge energy of approximately 7127 eV, confirming an iron oxidation state of +3 for all samples. Based on the

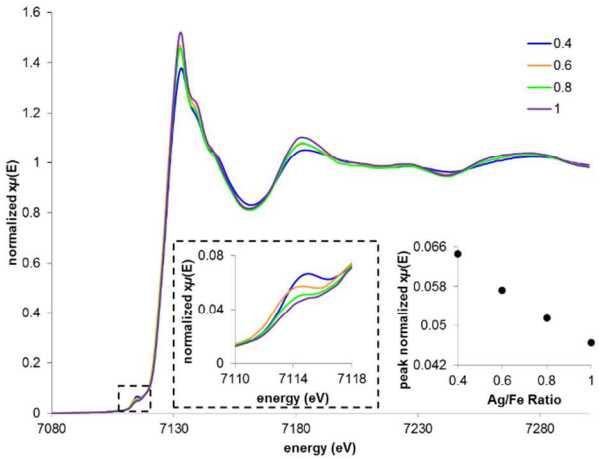

Figure 4. X-ray absorption spectroscopy (Fe K-edge) of as prepared samples. Dotted line region used for inset.

XAS data, the average iron oxidation state does not vary to any significant extent, since the Fe-edge energies range by < 0.1 eV (between 7126.9 and 7127.4 eV) and no direct correlation between silver content (Ag/Fe ratio) and Fe edge position is observed, **Figure 4**. A plot of EXAFS data in radial space shows no significant change up to 3.0 Å as a function of Ag content. However, the Fe-Ag scattering path (3.0-3.5 Å) changes as a function of silver concentration, Figure S2.

The normalized absorbance intensity of the iron pre-edge peak decreases linearly as the amount of silver in the delafossite samples increases, **Figure 4, inset**. The decrease in intensity and change in appearance of the pre-edge peak from silver deficient to stoichiometric $AgFeO_2$ would generally be attributed to a slight change in either the oxidation state of iron, the coordination environment of iron, or a combination of the two.[11,12] It is evident that oxidation state of iron is not changing after examination of the iron K-edge. A variety of iron-containing minerals have been shown to demonstrate more intense pre-edge peaks for coordination numbers of 4 or 5 and lower pre-edge absorption for 6-coordinate iron in the 3+ oxidation state.[12] Silver ferrite is composed of layers of FeO_6 octahedra and would be expected to have a pre-edge peak of relatively low intensity. While pre-edge peaks in octahedral transition metal complexes are ordinarily resultant of forbidden 1s→3d electronic transitions, such transitions are allowed when the local symmetry is distorted, commonly observed in octahedral iron-containing compounds owing to facile 3d→4p orbital mixing.[11,13] Further, the Raman data indicate the presence of a non-crystalline maghemite, γ-Fe_2O_3, phase which is a spinel structure comprised of both tetrahedral and octahedral Fe^{3+}. The tetrahedral Fe^{3+} in γ-Fe_2O_3 contributes to an increase in pre-edge intensity compared to exclusively octahedral Fe^{3+}.[14] The pre-edge intensity increases with decreasing Ag/Fe ratio, correlating with an increasing amount of maghemite present as indicated by the Raman spectra. XANES data at the Ag K-edge were also collected and silver was determined to be in the +1 oxidation state, where absorption spectra in the XANES region were indistinguishable for all Ag/Fe ratios. Thus, the XANES results indicate that the silver and iron oxidation states do not change as a function of crystallite size. In addition, iron experiences a difference in the pre-edge region which is consistent with the presence of maghemite in silver ferrite samples with apparent silver deficiency.

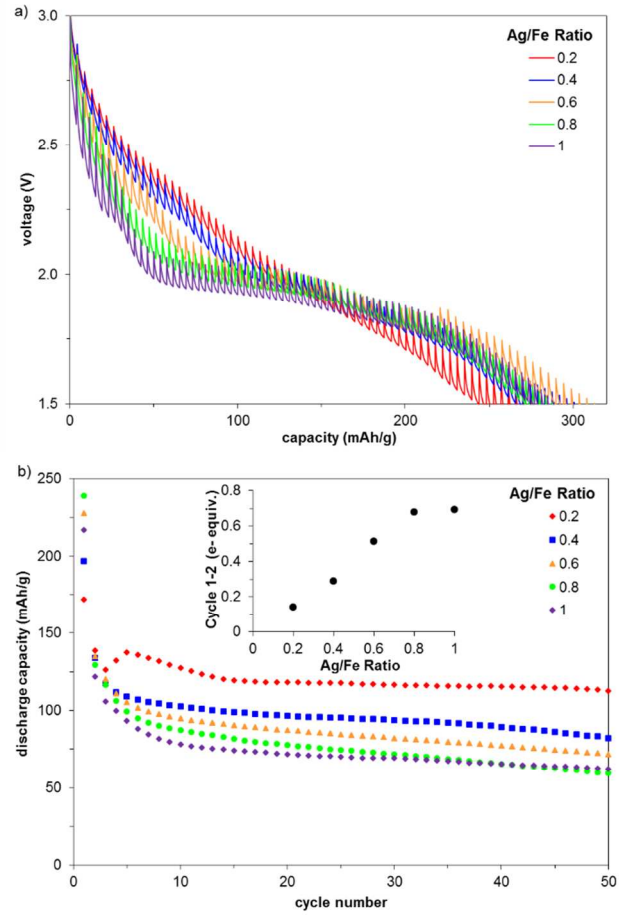

Figure 5. Testing of Li/silver ferrite based electrochemical cells. **a.** Voltage versus capacity on galvanostatic intermittent titration-type test. **b.** Discharge capacity versus cycle number. Inset shows difference between Cycle 1 and Cycle 2, in units of electron equivalents.

To examine the electrochemical behaviour of silver ferrite cathodes, two electrode cells with lithium anodes and 1 M $LiPF_6$ in ethylene carbonate/dimethyl carbonate electrolyte were utilized. Galvanostatic intermittent titration technique (GITT) type testing was employed with intermittent discharge (0.006 mA/cm^2) followed by open circuit rest. Significant differences in polarization were evident among the silver ferrite samples upon initial reduction, where the low silver/small crystallite size, high surface area material showed both higher operating voltages and decreased polarization during the initial stage of discharge, **Figure 5a**. The small crystallite, low silver materials demonstrate a sloped voltage profile throughout the discharge. The high silver (Ag/Fe = 1.0) material shows a steep voltage change to 2.0 V followed by a broad plateau. The length of the 2.0 V plateau decreases with decreasing crystallite size and silver content. Galvanostatic cycling was conducted using discharge and charge rates of 0.15 mA/cm^2 between voltage limits of 1.5 and 3.5 V. The delivered discharge capacities over 50 cycles are shown, **Figure 5b**. There is a significant change in capacity between cycles 1 and 2 where the change in capacity is directly proportional to the Ag^+ content in the silver ferrite when considered with respect to electron equivalents, **Figure 5b, inset.** Between cycles 10 and 50 the discharge capacities show only gradual fade, indicating that the discharge-charge

process is reversible for this system. Notably, the silver ferrite sample with the lowest silver content, x = 0.2, and smallest crystallite size delivers the highest capacity, ~200% that of stoichiometric $AgFeO_2$, and demonstrates the lowest capacity fade of the group. For comparison, pure maghemite (γ-Fe_2O_3) was tested as a cathode material. Lithium/maghemite cells tested under galvanostatic cycling yielded 80 mAh/g on cycle 1 fading to 60 mAh/g in following cycles, far lower than the 130 mAh/g demonstrated by the 0.2/1.0 silver to iron ratio material. Thus, maghemite alone is not responsible for the significant increase in delivered capacity in the low silver content small crystallite size silver ferrite material.

The electrochemical results are consistent with reduction of silver ion, Ag^+, to silver metal, Ag^0, and reduction of Fe^{3+} to Fe^{2+} during the initial discharge. The reduction of Ag^+, to silver metal, Ag^0, a displacement reaction, would be expected to result in higher polarization which is observed for the higher silver containing samples in the GITT type testing. It should be noted that the small crystallite size low sliver content materials have higher surface area which also contributes to lower polarization. Under cycling tests, the difference in capacity between cycle 1 discharge and cycle 2 discharge scales with silver content, **Figure 5b, inset** where the higher silver containing materials show greater capacity change between cycle 1 and cycle 2. These results imply that once formed, a portion of the silver metal is no longer electrochemically active. The electrochemical behaviour of the samples was explored by slow scan cyclic voltammetry. The first cathodic scan showed a large irreversible peak near 2.0 V. Subsequent scans displayed lower current reversible peaks, Figure S3, consistent with the cycling data.

Conclusions

The synthetic approach demonstrated herein provides a new paradigm for composite synthesis, which may be applicable toward new materials with energy or energy storage applications. Limiting the initial concentration of a single reagent provided synthetic control of silver ferrite of crystallite size; x-ray powder diffraction confirmed a silver ferrite crystallographic structure with systematic variation of crystallite size across the compositional series. However, with this report, the composite nature of the low silver materials as a combination of crystalline silver ferrite, $AgFeO_2$, and non-crystalline maghemite γ-Fe_2O_3 was established by Raman spectroscopic and x-ray absorption analyses. Further, as a cathode, the low silver content composites exhibited profound electrochemical capacities ~200% higher relative to stoichiometric silver ferrite samples.

Acknowledgements

The authors acknowledge the Department of Energy (DOE), Office of Basic Energy Sciences (BES), under Grant DE-SC0008512. K. Kirshenbaum acknowledges the Gertrude and Maurice Goldhaber Distinguished Fellowship Program. X-ray absorption spectra were collected on beam line X11A at Brookhaven National Laboratory's National Synchrotron Light Source (NSLS), supported by the DOE, Office of Science, BES, under Contract No. DE-AC02-98CH10886. The authors acknowledge K. Pandya for assistance with XAS.

Notes and references

[a] Department of Chemistry, Stony Brook University, Stony Brook, NY 11794-3400. *Email: kenneth.takeuchi.1@stonybrook.edu.
[b] Brookhaven National Laboratory, Upton, NY 11973-5000.
[c] Department of Materials Science and Engineering, Stony Brook University, Stony Brook, NY 11794-2275.

1(a) R. D. Shannon, D. B. Rogers and C. T. Prewitt, *Inorganic Chemistry*, 1971, **10**, 713; (b) M. A. Marquardt, N. A. Ashmore and D. P. Cann, *Thin Solid Films*, 2006, **496**, 146.
2 A. Krause and K. Pilawski, *Zeitschrift fur Anorganische und Allgemeine Chemie*, 1931, **197**, 301.
3(a) A. Krause and A. Lewandowski, *Zeitschrift fur Anorganische und Allgemeine Chemie*, 1972, **389**, 71; (b) Y.-J. Shin, J.-H. Kwak and S. Yoon, *Bulletin of the Korean Chemical Society*, 1997, **18**, 775; (c) T. Ishiguro, A. Kitawaza, N. Mitzutani and M. Kato, *Journal of Solid State Chemistry*, 1981, **40**, 170; (d) M. Tanaka, M. Hasegawa, T. Higuchi, T. Tsukamoto, Y. Tezuka, S. Shin and H. Takei, *Physica B*, 1998, **245**, 157; (e) R. Berthelot, M. Pollet, J.-P. Doumerc and C. Delmas, *Inorganic Chemistry*, 2011, **50**, 4529; (f) S. Ouyang, D. Chen, D. Wang, Z. Li, J. Ye and Z. Zou, *Crystal Growth and Design*, 2010, **10**, 2921; (g) Y. L. N. Murthy, T. K. Rao, I. V. K. Viswanath and R. Singh, *Journal of Magnetism and Magnetic Materials*, 2010, **322**, 2071; (h) S. Kumar, S. Marinel, M. Miclau and C. Martin, *Materials Letters*, 2012, **70**, 40.
4 K. E. Farley, A. C. Marschilok, E. S. Takeuchi and K. J. Takeuchi, *Electrochemical and Solid-State Letters*, 2012, **15**, A23.
5 S. Krehula and S. Music, *Journal of Molecular Structure*, 2013, **1044**, 221.
6 Y. Dong, C. Cao, Y.-S. Chui and J. A. Zapien, *Chemical Communications (Cambridge, United Kingdom)*, 2014, **50**, 10151.
7 F. Sauvage, D. Muñoz-Rojas, K. R. Poeppelmeier and N. Casañ-Pastor, *Journal of Solid State Chemistry*, 2009, **182**, 374.
8(a) K. J. Takeuchi, S. Z. Yau, M. C. Menard, A. C. Marschilok and E. S. Takeuchi, *ACS Applied Materials and Interfaces*, 2012, **4**, 5547; (b) K. J. Takeuchi, S. Z. Yau, A. Subramanian, A. C. Marschilok and E. S. Takeuchi, *Journal of the Electrochemical Society*, 2013, **160**, A3090; (c) S. Zhu, A. C. Marschilok, E. S. Takeuchi and K. J. Takeuchi, *Electrochemical and Solid-State Letters*, 2009, **12**, A91; (d) A. C. Marschilok, E. S. Kozarsky, K. Tanzil, S. Zhu, K. J. Takeuchi and E. S. Takeuchi, *Journal of Power Sources*, 2010, **195**, 6839; (e) M. C. Menard, A. C. Marschilok, K. J. Takeuchi and E. S. Takeuchi, *Electrochimica Acta*, 2013, **94**, 320.
9(a) W. C. Sheets, E. Mugnier, A. Barnabe, T. J. Marks and K. R. Poeppelmeier, *Chemistry of Materials*, 2006, **18**, 7; (b) A. Winchainchai, P. Dordor, J. P. Doumerc, E. Marquestaut, M. Pouchard and P. Hagenmuller, *Journal of Solid State Chemistry*, 1988, **74**, 126; (c) J. E. Clayton, D. P. Cann and N. Ashmore, *Thin Solid Films*, 2002, **411**, 140; (d) R. Nagarajan and N. Tomar, *Journal of Solid State Chemistry*, 2009, **182**, 1283; (e) D. Y. Shahriari, N. Erdman, U. T. M. Haug, M. C. Zarzyczny, L. D. Marks and K. R. Poeppelmeier, *Journal of Physics and Chemistry of Solids*, 2003, **64**, 1437.
10(a) M. I. Dar and S. A. Shivashankar, *RSC Advances*, 2014, **4**, 4105; (b) N. S. Chaudhari, S. S. Warule, S. Muduli, B. B. Kale, S. Jouen, B. Lefez, B. Hannoyer and S. B. Ogale, *Dalton Transactions*, 2011, **40**, 8003.
11 T. E. Westre, P. Kennepohl, J. G. DeWitt, B. Hedman, K. O. Hodgson and E. I. Solomon, *J. Am. Chem. Soc.*, 1997, **119**, 6297.
12 M. Wilke, F. Farges, P.-E. Petit, G. E. Brown, Jr. and F. Martin, *American Mineralogist*, 2001, **86**, 714.
13(a) R. G. Shulman, Y. Yafet, P. Eisenberger and W. E. Blumberg, *Proceedings of the National Academy of Sciences*, 1976, **73**, 1384; (b) G. Calas and J. Petiau, *Solid State Communications*, 1983, **48**, 625; (c) G. A. Waychunas, *American Mineralogist*, 1987, **72**, 89.
14 D. Lützenkirchen-Hecht, R. Wagner, S. Bieder and R. Frahm, *Journal of Physics: Conference Series*, 2013, **425**, 132006.